Ceramics-Silikáty 66 (3), 354-364 (2021)
www.ceramics-silikaty.cz doi: 10.13168/cs.2022.0031

IMPEDANCE SPECTROSCOPY AND PERMITTIVITY STUDY OF (1-x)NBT-xBT CERAMICS

#M.MESRAR, A. ELBASSET, F. ABDI, N-S. ECHATOUI, T. LAMCHARFI

Signals, Systems and Components Laboratory (LSSC), Faculty of Sciences and Technologies of Fez, Sidi Mohamed Ben Abdellah University, B.P. 2022, Fez, Morocco

#E-mail: mohammed.mesrar@usmba.ac.ma

Submitted June 8, 2022; accepted July 11. 2022

Keywords: (1-x)($Na_{0.5}Bi_{0.5}$)$TiO_{3-x}BaTiO_3$, Solid-state method, Rietveld refinement, Complex impedance, Cole-Cole diagram

The complex impedance spectroscopy method was applied to evaluate the profound characteristics of the electrical transport capacity of lead-free ferroelectric ceramic solid solutions of (1-x)($Na_{0.5}Bi_{0.5}$)TiO_{3-x}Ba TiO_3 (NBT-xBT) (0.00 ≤ x ≤ 0.10). The elaboration of NBT-xBT, via a solid-state reaction between ($Na_{0.5}Bi_{0.5}$)TiO_3 and $BaTiO_3$, was determined using X-ray diffraction. Refinements, at room temperature, identified a rhombohedral phase, space group R3c for x = 0.0 and 0.03, which possesses an antiphase, corresponding to the tilting system ā ā ā with an angle of inclination of 8.24° according to Glazer's notation. We used the complex impedance, complex electric Cole-Cole diagram and frequency-dependent AC conductivity analysis to examine the relaxation and conduction mechanism in these samples, which exhibit non-Debye type behaviour. In addition, using an equivalent circuit composed of resistance and capacitance, we examined the different contributions (grains and grain boundaries) in our samples. ($Na_{0.5}Bi_{0.5}$)TiO_3 exhibits a dielectric resonance, which manifests itself as negative permittivity. The resonance development of NBT-xBT in the range (500 Hz − 2 MHz) is discussed in this paper.

INTRODUCTION

Over the last few years, environmental concerns have intensified due to global warming and climate change. Therefore, it is highly recommended to design non-toxic components to eliminate lead-based ferroelectric materials in different equipment, such as transducers, actuators, multilayer capacitors and filters [1, 2]. Since bismuth is comparable to lead in the outermost electron layer and mass, it is a likely candidate to be a substitute for lead in ferroelectric substances [3, 4]. The material ($Na_{0.5}Bi_{0.5}$)TiO_3 (NBT) was first found in 1960 by Smolensky et al. [5]. It is currently the most likely successor material to lead-based compounds, such as Pb(Zr,Ti)O_3, which exhibits very good piezoelectric characteristics near the morphotropic phase boundary. Furthermore, NBT's high-temperature ionic conductivity has variously been treated according to the intended application. Due to its high conductivity, NBT is considered a very good conductor of oxide ions for industrial uses in sensor devices and electrochemistry[6]. However, for ferroelectric and energy storage applications, this conductivity is perceived as a constraint [7]. Many studies have investigated rare earth-doped NBT products to solve these problems [8-10]. In this work, we found that a small substitution of Barium in the A-site of the NBT compound resulted in an increase in the dielectric constant and a shift in the T_m position towards higher temperatures, which is an advantage for energy storage capacitors operating at high temperatures [11]. The control of the electrical transport behaviour and clarification of its operation, in particular at high temperatures, are elements to be taken into account before any implementation. The impedance spectroscopy method has also been widely used to study both localised (dipolar) relaxation and delocalised (long-range) conduction of ferroelectric compounds. Furthermore, thanks to this impedance spectroscopic approach, a certain relationship between the microstructure (presence of grains and grain boundaries) and the characteristics of ferroelectric compounds can be established[12-14].

Benyoussef et al. [8, 10] conducted complex impedance and spectroscopic analyses of the modulus of NBT and reported the presence of grains and grain boundary contributions in the NBT. To evaluate the contribution of the grains and grain boundaries, the researchers applied an equivalent circuit to model the electrical behaviour of these materials. In addition, J. East et al. [15] investigated the impedance and modulus spectroscopy of (1-x)NBT-xBT between room temperature (RT) and 500 °C as well as reported on the presence of a grain effect in the material. Although this impedance spectroscopy technique has been used to determine the electrical characteristics of (1-x)NBT-xBT, a systematic study of ceramics over the full compositional range (0.0 ≤ x ≤ 0.10) is not available in the literature.

In the present investigation, the NBT was produced using a solid phase reaction approach. Moreover, the dielectric properties of the materials were determined using the Cole-Cole model. We also examined the presence of a negative dielectric constant as a function of the frequency as well as the electrical properties. We also found that the resonance frequency of the NBT shifts as a function of the measurement frequency. The excellent electrical and piezoelectric properties make these materials ideally suited for the manufacture of ferroelectric components.

EXPERIMENTAL

$(1\text{-}x)(Na_{0.5}Bi_{0.5})TiO_{3\text{-}x}BaTiO_3$ ($0.00 \leq x \leq 0.10$) were synthesised by a high temperature solid- state reaction. As the reaction, the process in the solid state is related to the diffusion capacity of the cations and anions in the solid state, where such processes require long reaction times and high temperatures to increase the diffusion rate, which, in turn, increases the reaction rate to obtain a stable phase. The stoichiometric proportions of Na_2CO_3, Bi_2O_3, TiO_2 and $BaCO_3$ were ground for 60 minutes in an agate mortar. After grinding, the product was homogenised in a container in the presence of acetone for 4 hours. The powder obtained was first calcined at 1000 °C for 4 hours, then ground with an agate mortar for 30 minutes. The various powdered materials were mixed with a 3 % Polyvinyl alcohol (PVA) binder and pressed into 10 mm in diameter cylindrical pellets at a pressure of 8 $t \cdot cm^{-2}$ using a manual press. The pellets were sintered at 1100 °C for 4 hours in a resistance furnace. The crystallographic phases were performed by X-ray diffraction (X'pert Pro PANalytical) using (CuKα = 1.5406 Å) radiation at room temperature in an angular range of 2θ: 20 – 80°. The crystallite sizes and lattice constants were obtained from the Rietveld refinements of the recorded diffraction data. The dielectric parameters, such as the dissipation factor, capacitance, phase angle and impedance, were calculated over a wide frequency range from 500 Hz to 2 MHz at different temperatures (40 − 600 °C) using an impedance analyser (Agilent 4284A) connected to a computer.

RESULTS AND DISCUSSION

Refinement and structural characterisation

The Rietveld technique was applied to refine the crystallographic structures with an increasing Ba^{2+} concentration in the solid solution samples. All the samples were examined using Rietveld's refinement software FullProf integrated with WinPlotr. [16] The peak profile was represented by a pseudo-Voigt function. In particular, the background level was defined through a polynomial function with 12 coefficients. The refined factors were as follows: fractional atomic coordinates (x, y, z), a scale coefficient, atomic occupancy, a preferential orientation coefficient, an isotropic displacement coefficient in Å2, a zero-point detector, global isotropic displacement parameters (temperature), cell coefficients (a, b, c, α, β, γ), a background refinement using a 12-coefficient polynomial function, half-width coefficients (u, v, w), asymmetry coefficients, and a profile shape coefficient (η).

For the (1-x)NBT-xBT samples with ($0.00 \leq x \leq 0.10$), the refinements were carried out considering rhombohedral symmetry (R3c). According to this model, Na^+, Bi^{3+} and Ba^{2+} are located at sites 6a (0, 0, z), the Ti^{4+} cations are also located at positions 6a (0, 0, z) and the oxygen atoms are located at the basic positions so that 18b (x, y, z). In the case of the refinement of samples higher than (x = 7 %), it was conducted by admitting tetragonal symmetry. Figure 1a shows the typical Rietveld refinement patterns as well as the spectra of the different samples obtained at room temperature for the (1-x)NBT-xBT ceramics calcined at 1000 °C for 4 hours. The representation of the lattice parameters by the Diamond 4.0 software [17], which allowed us to observe the cationic displacements within the A site, thus the cations (Na^+/Bi^{3+}) are not located at the centre of the cuboctahedral and octahedral cavities (Figure 1b). Based on the model proposed by P. Thomas et al. [18], these displacements are of a polar axis direction [111] p-equivalent to the axis (c) of the combined hexagonal mesh of the adjacent oxygen octahedra, which corresponds to the tilts system $\bar{a}\ \bar{a}\ \bar{a}$ with an inclination angle of 8.24° according to the notation of Glazer. [19]

Table 1 shows, in detail, the atomic occupancies for the different compounds. The Ti^{4+} cations are found in an octahedral environment; the Ti-O distances have short and long lengths resulting in distorted octahedra, the average Ti^{4+}-O distance is around 1.97 Å. Indeed, these octahedra have successive connections and extensions in three dimensions. The results of the determination of the various inter-atomic distances (Table 2) indicate that the Na/Bi/Ba atoms constitute $(Na/Bi/Ba)O_{12}$ polyhedra, the average distance of the Na/Bi/Ba-O bonds is estimated at approximately 2.69 Å.

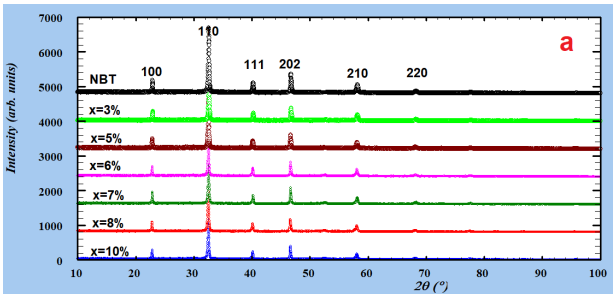

a) X-ray diffraction pattern of all the sintered (1-x)NBT-xBT ceramics.

Figure 1. X-ray diffraction pattern.

continue on the next page ...

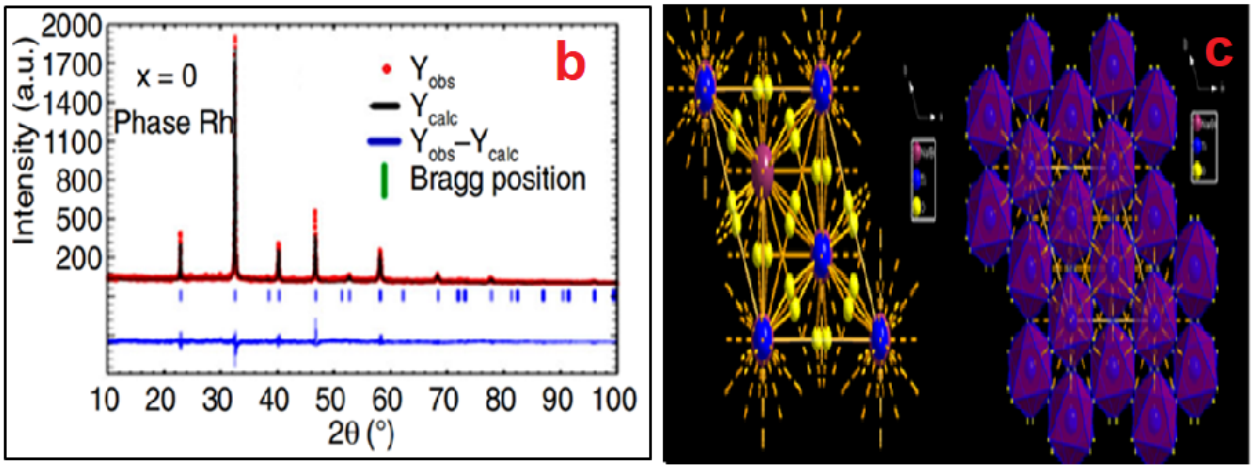

Figure 1. X-ray powder diffraction pattern by Rietveld refinement of (b) 0.95NBT-0.05BT and (c) 0.95NBT-0.05BT: experimental, calculated and their difference. The projection views of the structures are shown in the frame.[11]

Table 1. Results of the refined structural parameters of the (1-x)($Na_{0.5}Bi_{0.5}$)$TiO_{3-x}BaTiO_3$ samples.

Atom	Site	x	y	z	B(Å)	Occupancy
			NBT			
Na/Bi	6a	0	0	0.2634	0.79	0.5/0.5
Ti	6a	0	0	0.0071	0.47	1
O	18b	0.1272	0.2464	0.0621	1.91	1
			0.95NBT-0.05BT			
Na/Bi/Ba	6a	0	0	0.2644	0.71	0.5/0.49/0.01
Ti	6a	0	0	0.0059	0.41	1
O	18b	0.1271	0.2463	0.0629	1.85	1
			0.90NBT-0.1BT			
Na/Bi/Ba	6a	0	0	0.2474	0.74	0.5/0.475/0.025
Ti	6a	0	0	0.0079	0.45	1
O	18b	0.1284	0.3340	0.0762	1.88	1

Table 2. Calculated inter-atomic distances (Å) and the O-Ti-O angles for the 0.95NBT-0.05BT compound.

0.95NBT-0.05BT			
3 × (Na/Bi/Ba)-O	2.871	3 × Ti-O	1.840
3 × (Na/Bi/Ba)-O	2.814	3 × Ti-O	2.001
3 × (Na/Bi/Ba)-O	2.523	<Ti-O>	1.970
3 × (Na/Bi/Ba)-O	2.729		
<(Na/Bi/Ba)-O>	2.690		
3 × O-Ti-O	165.840	3 × O-Ti-O	90.11
3 × O-Ti-O	94.130	3 × O-Ti-O	91.41

Dielectric investigations

In the present study, we examined the evolution of the dielectric properties of the different compositions of the (1-x)NBT-xBT system as a function of frequency for different temperatures in 20 °C steps. Dielectric measurements were performed on the (1-x)NBT-xBT pellets (12 mm in diameter and about 1 mm thick), sintered at 1100 °C for 4 hours. These measurements used an Agilent 4284A impedance meter and a temperature-controlled furnace. A computer controls the overall system. Figure 2 shows the variation curves of the dielectric constant recorded for the (1-x)NBT-xBT samples for different substitution rates (x = 0.00; 0.03; 0.05; 0.06; 0.07; 0.08 and 0.10). We observed two anomalies noted A and B as a function of frequency for all the samples. For the pure NBT, as the frequency increases, the dielectric constant steadily increases, then, in the vicinity of the noted anomaly A, it increases and passes through a maximum, corresponding to the so-called resonance frequency (*fr*), at this frequency to then decrease rapidly for a frequency close to anomaly B, known as the anti-resonance (*fa*). The value of the resonance frequency makes it possible to determine the frequency at which the dipole moment vector changes direction. This behaviour remains similar for all the compounds at different xBa^{2+} concentrations. On the other hand, these anomalies have been reported by El Basset et al [20] for the $Ba_{1-x}Sr_xTiO_3$.

As the temperature increases, the position of anomaly A shifts towards the low frequencies until a temperature T = 350 °C where an inverse shift of the resonance frequency (*fr*) towards the high frequencies is observed. It can also be noted that the maximum value of the dielectric permittivity increases with the temperature and reaches a maximum value at T = 350 °C

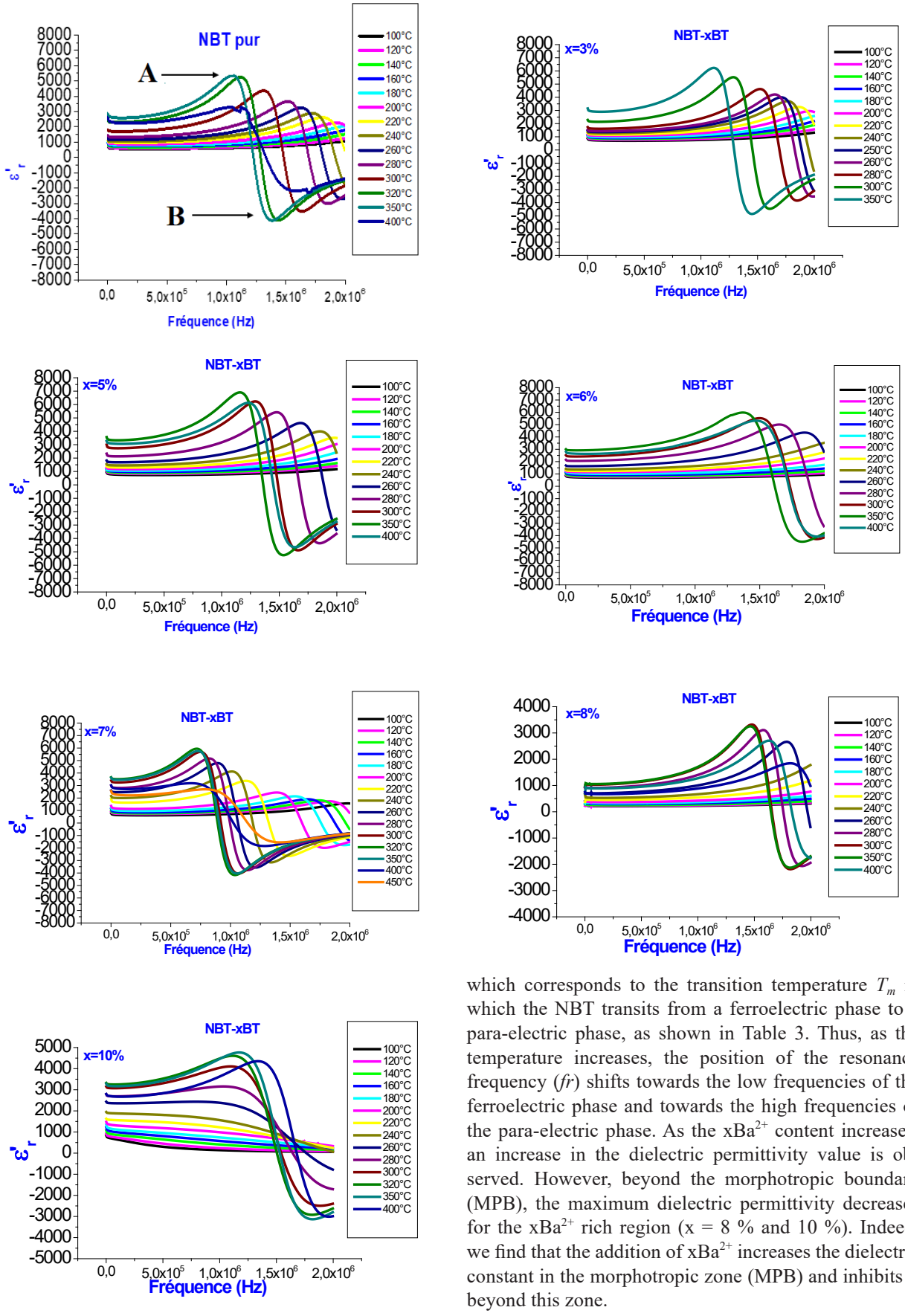

which corresponds to the transition temperature T_m in which the NBT transits from a ferroelectric phase to a para-electric phase, as shown in Table 3. Thus, as the temperature increases, the position of the resonance frequency (*fr*) shifts towards the low frequencies of the ferroelectric phase and towards the high frequencies of the para-electric phase. As the xBa^{2+} content increases, an increase in the dielectric permittivity value is observed. However, beyond the morphotropic boundary (MPB), the maximum dielectric permittivity decreases for the xBa^{2+} rich region (x = 8 % and 10 %). Indeed, we find that the addition of xBa^{2+} increases the dielectric constant in the morphotropic zone (MPB) and inhibits it beyond this zone.

Figure 2. The real part ε'_r of the complex permittivity of the (1-x)NBT-xBT samples sintered at 1100 °C for 4 hours. [11]

Table 3. The resonant frequency and permittivity of the (1-x)NBT-xBT samples at different temperatures.

T (°C)	NBT		3%		5%		6%		7%		8%		10%	
	fr (MHz)	εr	fr (MHz)	εr	fr (MHz)	εr	fr (MHz)	εr	fr (MHz)	εr	fr (MHz)	εr	fr (MHz)	εr
180	1.996	2042	-	-	-	-	-	-	-	-	-	-	-	-
200	1.911	2319	1.954	3071	-	-	-	-	-	-	-	-	-	-
220	1.817	2760	1.875	3397	.1.964	3597	-	-	1.913	2994	-	-	-	-
240	1.721	2912	1.766	3863	1.868	3959	-	-	1.727	3744	-	-	-	-
260	1.618	3283	1.637	4328	1.682	4735	1.860	4814	1.458	4992	1.785	2717	1.138	2286
280	1.582	3678	1.516	4747	1.477	5510	1.670	5743	1.240	5242	1.585	3055	1.157	3169
300	1.341	4391	1.292	5537	1.304	6338	1.516	5943	1.125	6992	1.490	3368	1.122	4087
320	1.118	5143	-	-	-	-	-	-	1.074	7009	-	-	1.131	4611
350	1.042	5384	1.106	6330	1.160	7060	1.375	6441	1.038	6597	1.458	3247	1.208	4807
400	1.183	3203	-	-	1.247	6131	1.447	5341	1.118	2893	1.637	2717	1.381	4382

On the other hand, Belhajji et al [21] observed the same behaviour with regards to the permittivity as a function of the frequency, relating this shift in the $T \geq 505$ °C range by the probable competition between the thermal energy and applied electric field. Moreover, this displacement phenomenon of the resonance frequency to low frequencies ($T \leq 350$ °C) and the increase in the dielectric constant in this temperature range can be due to a particular process of polarisation related to the increase in the number of dipoles or, more precisely, to the increase in the number of dipolar orientations governed by the decrease in the degree of dipolar disorder in the ferroelectric phase. The incorporation of Ba^{2+} into the (1-x)NBT-xBT ceramics leads to the generation of oxygen vacancies at high frequency and the effect of free electrons will be strongly dominated and it overcomes the effect of the bound charges and this is manifested, under the effect of an external electric field, where the extended electrons will oscillate collectively, inducing a dipole rich state. Due to the presence of the free and bound charge carriers in the sample, the (1-x)NBT-xBT ceramics evolve from a dielectric to a metal with a frequency.

Complex impedance spectroscopy (CIS)

Variation of real part of impedance (Z′) with frequency

For many polycrystalline dielectric ceramics, useful information can be obtained from the impedance (Z^*), where the real part (resistive part Z') and the imaginary part (capacitive part Z'') are related as follows:

$$Z^*(\omega) = Z'Z''/(Z' + Z'') \quad (1)$$

Figure 3. shows the variation of the real part of the impedance (Z') with the frequency at different temperatures for the (1-x)NBT-xBT samples for the different substitution rates (x = 0.00; 0.03; 0.05; 0.06; 0.07; 0.08 and 0.10). As shown in the figure, the Z' values increase with the increasing frequency, showing a Z'_{max} at low frequencies, and then they gradually decrease and become relatively independent of the frequency. Furthermore, the maximum value of Z'_{max} at low frequencies suggests that all types of polarisation are present. [22-24]

For the (1-x)NBT-xBT system with ($0.00 \leq x \leq 0.10$), we observed a decrease in Z'max as a function of the measurement temperature until reaching a temperature of $T = 350$ °C. Whereas in the interval, $T > 350$ °C, we

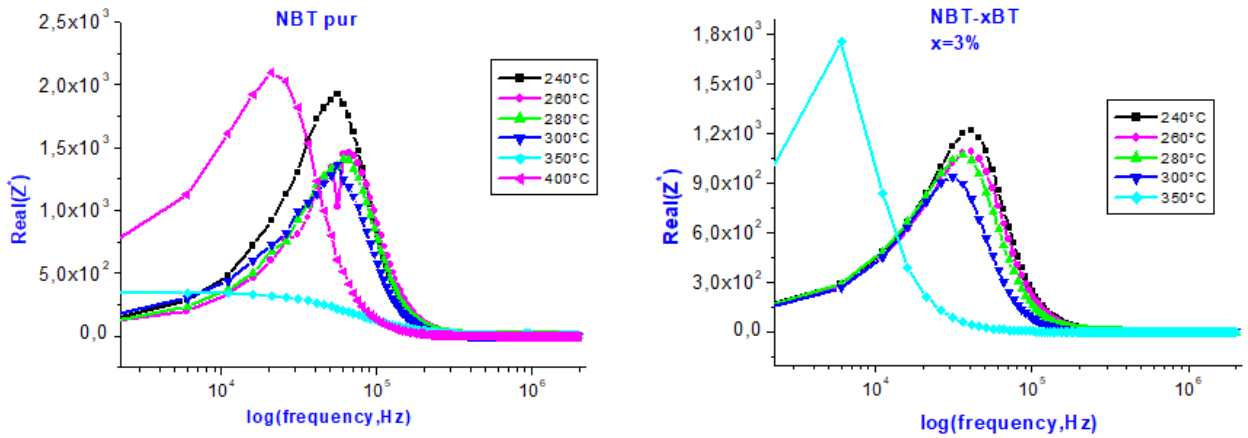

Figure 3. Real part (Z') versus the frequency curves for the (1-x)NBT-xBT system.

continue on the next page ...

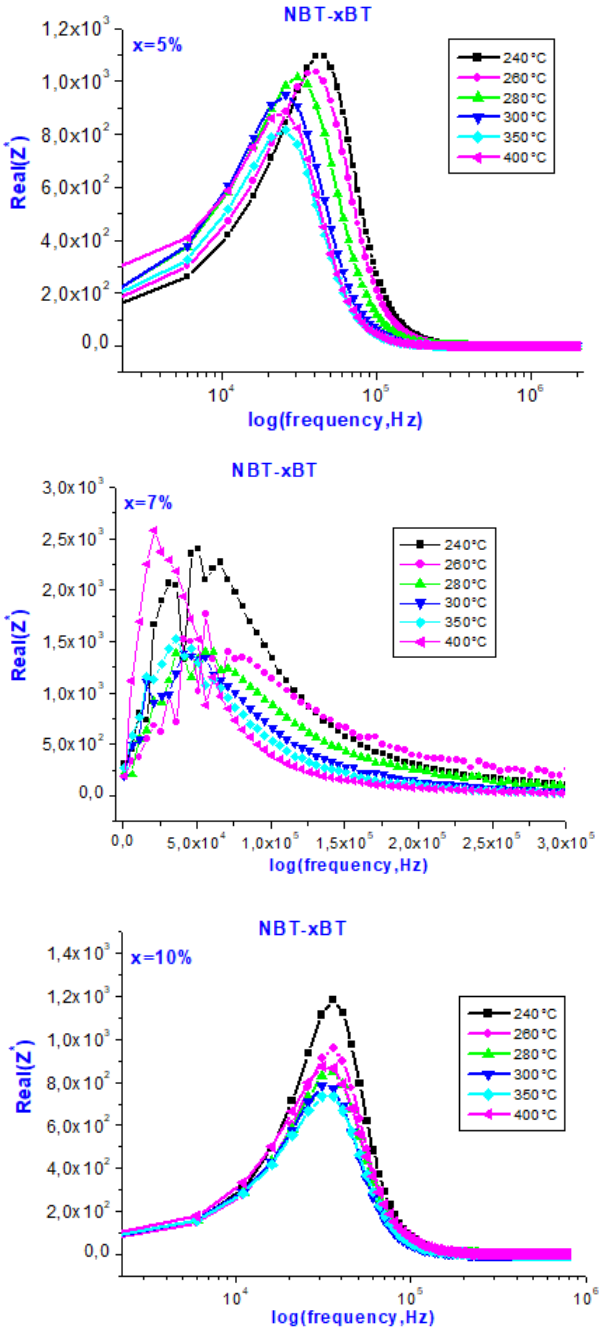

Figure 3. Real part (Z') versus the frequency curves for the (1-x)NBT-xBT system.

observed the opposite evolution (there is an increase in the Z'max value). The temperature of T = 350 °C corresponds to the transition temperature T_m at which $(Na_{0.5}Bi_{0.5})TiO_3$ transits from the ferroelectric phase to the paraelectric phase. This decrease in Z'max with the increasing temperature suggests high-temperature conduction behaviour. [25] Furthermore, for ceramics (0 % ≤ x ≤ 5 %), a shift in the maximum frequency (f_{max}) from Z'_{max} to low frequencies is observed. However, at x = 6 %, the maximum frequency shifts towards the high frequencies, as mentioned in Table 4. As the xBT doping

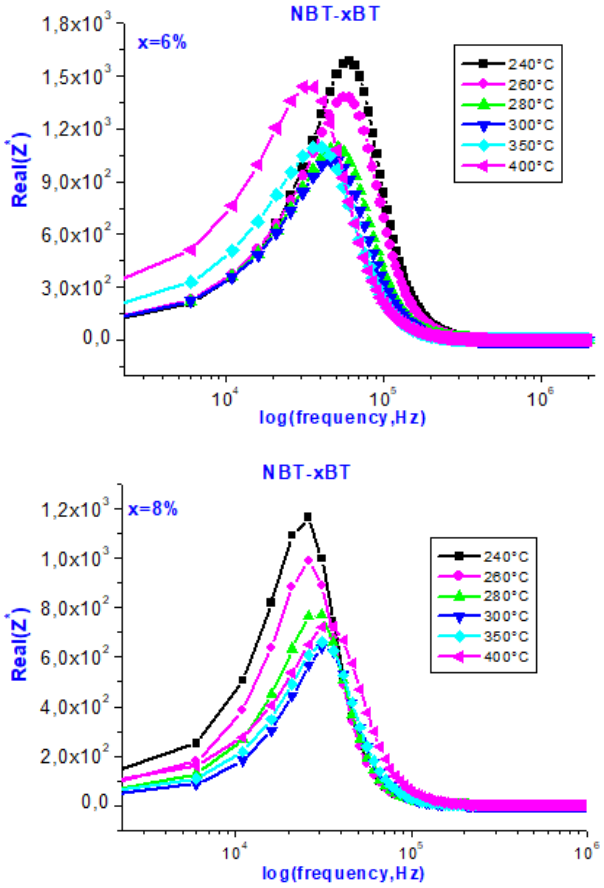

Table 4. Amplitude values of Z' maxima with frequency f_{max}.

xBa^{2+}	0 %	3 %	5 %	6 %	7 %	8 %	10 %
Z'$_{max}$	1352	936	942	1012	1398	631	725
f_{max} (Log(frequency, KHz))	55.10	30.15	26.20	46.98	49.87	31.81	36.02

rate increases and for a given temperature at T = 300 °C, a decrease in the amplitude of Z' is observed with a shift in the position (f_{max}) towards the low frequencies (Figure 4). The decrease in the amplitude of Z' maxima with the increasing Ba content indicates an increasing loss in the resistive property of the samples and leads to an increase in the conductivity.

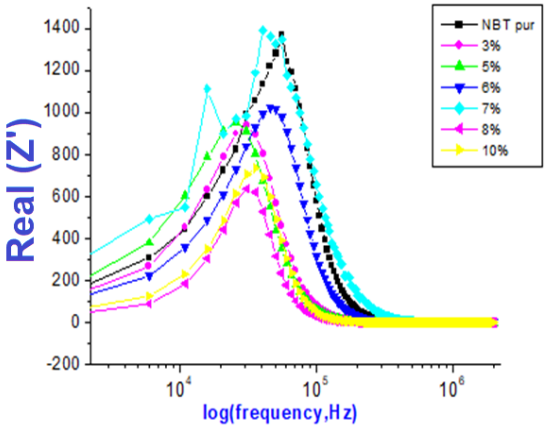

Figure 4. Variation of Z'_{max} as a function of the xBT doping content at T = 300 °C.

Variation of imaginary part of impedance (Z") with frequency

Figure 5 shows the variation in the imaginary part of the impedance (Z'') with the frequency for the (1-x) NBT-xBT material with ($0.00 \leq x \leq 0.10$). A similar behaviour regarding the evolution of the real part of the impedance (Z') with the frequency was observed for all the compositions. The variation of Z'' as a function of frequency shows a maximum (Z''_{max}) for all the samples. The frequency at which Z'_{max} is observed is designated as the relaxation frequency ($\omega = 2\pi f_{max} = 1/\tau$). [11] For a given composition (x = 0.0), it is observed that (i) there is a decrease in the Z''_{max} value with a shift in the position (peak frequency $f_{max} = 1/\tau$) to lower frequencies with increasing temperature, as mentioned in Table 5. This implies that the relaxation time increases as well as that the relaxation process is thermally activated at higher temperatures. [12, 26] As the doping rate increases and beyond x = 7 %, the maximum of Z''_{max} shifts to higher frequencies, suggesting a lower relaxation time.

Table 5. Amplitude values of the Z'' maxima with the frequency f_{max}.

xBa^{2+}	0 %	3 %	5 %	6 %	7 %	8 %	10 %
Z'_{max}	4023	3101	2914	2712	3245	2945	2514
f_{max} (Log(frequency, KHz))	52.30	41.02	40.03	42.47	43.52	40.54	42.66

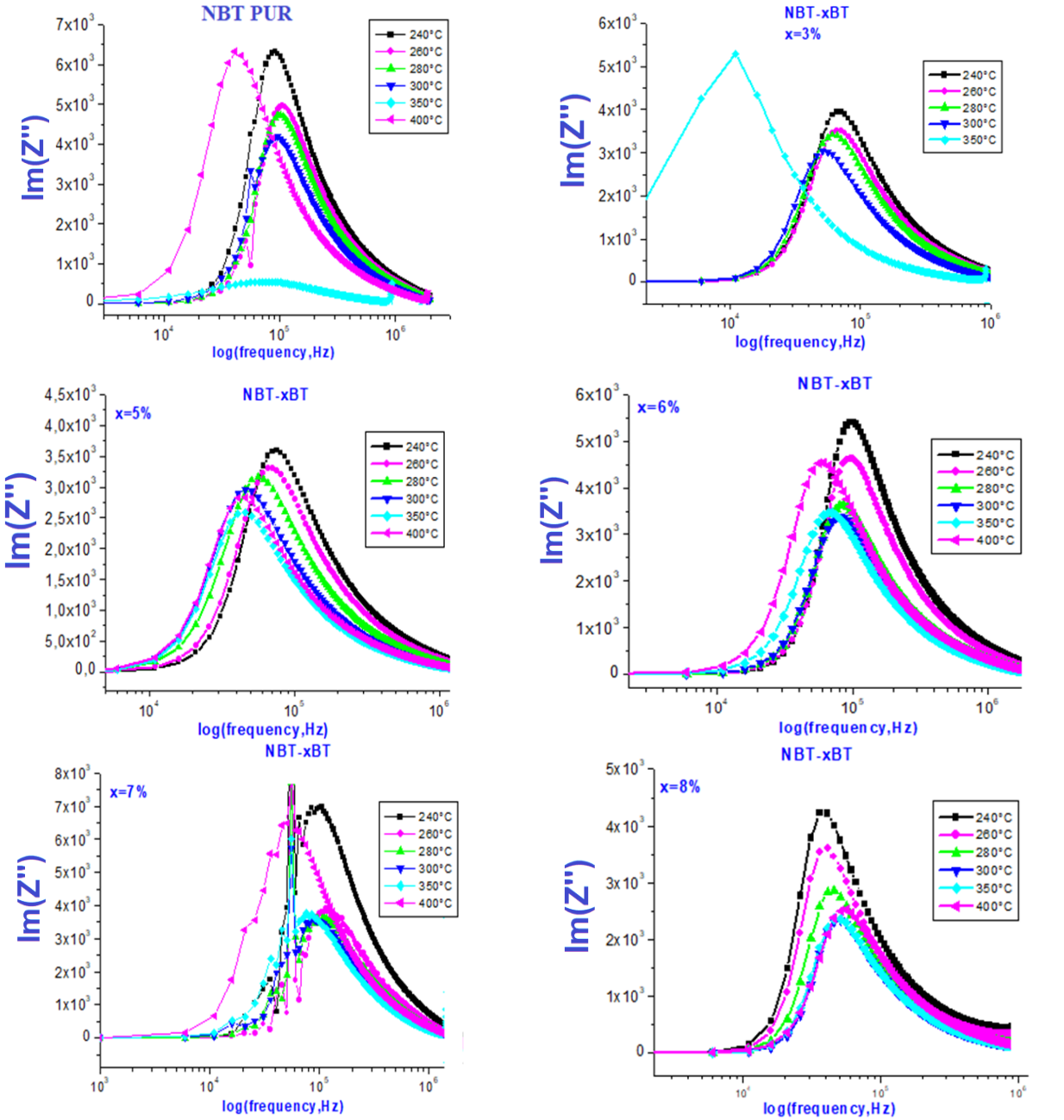

Figure 5. Imaginary part of the Z'' curves as a function of frequency for the (1-x)NBT-xBT system. *continue on the next page ...*

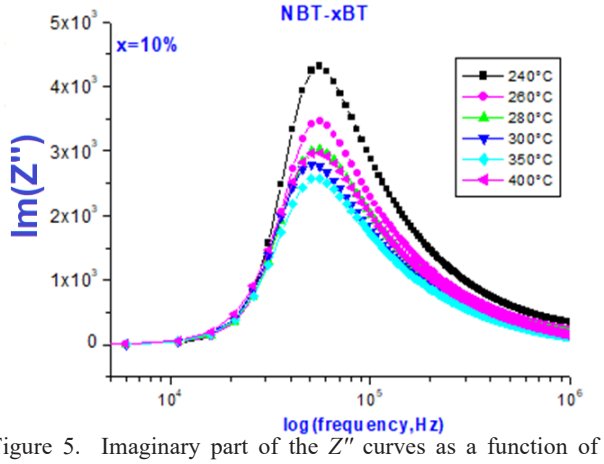

Figure 5. Imaginary part of the Z'' curves as a function of frequency for the (1-x)NBT-xBT system.

Furthermore, Ch Sameera Devi et al [7, 27] suggest that this behaviour is attributed to the space charge effect. Indeed, the relaxation frequency ($f_{max} = 1/\tau$) depends on both the temperature and the composition of xBT.

Modelling approach: the Cole–Cole plot

Figure 6 shows the Cole-Cole plot for the (1-x) NBT-xBT sample with the ($0.00 \leq x \leq 0.10$) system at several temperatures (240, 260, 280, 300, 350, 400 °C). Initially, at low temperatures, due to the high resistivity of the samples, the impedance measurements for all the samples below 240 °C did not show full semicircles or semi-circular arcs. Therefore, the impedance data for temperatures above or equal to 240 °C were taken into account for the equivalent circuit modelling to separate the resistances and capacitances of the grains and grain boundaries. The Cole-Cole spectra are characterised by semi-circular arcs and the intersection of these arcs with the axis of the reals allowed one to determine the strength of the material R. The values of C are obtained by applying the following relation: $\omega RC = 1$. Furthermore, the intersection at low frequency reveals the behaviour of the grain boundary (Rgb) and at high frequency the response of the grains (Rg). [28]

The obtained Cole-Cole plots are all arcs or semicircles for all the samples. Thus, the centre of the semicircles is below the real axis, which shows that the relaxation of the materials is not the Debye-type. [8, 29] This feature of the impedance spectra is almost similar at different temperatures and for all the compounds, while the radius of the semicircles (resistance) decreases with the increasing temperature until a critical temperature at $T = 350$ °C. Hence, above $T = 350$ °C, an inverse evolution is observed. This indicates that the conductivity of the samples increases with the temperature up to $T = 350$ °C.

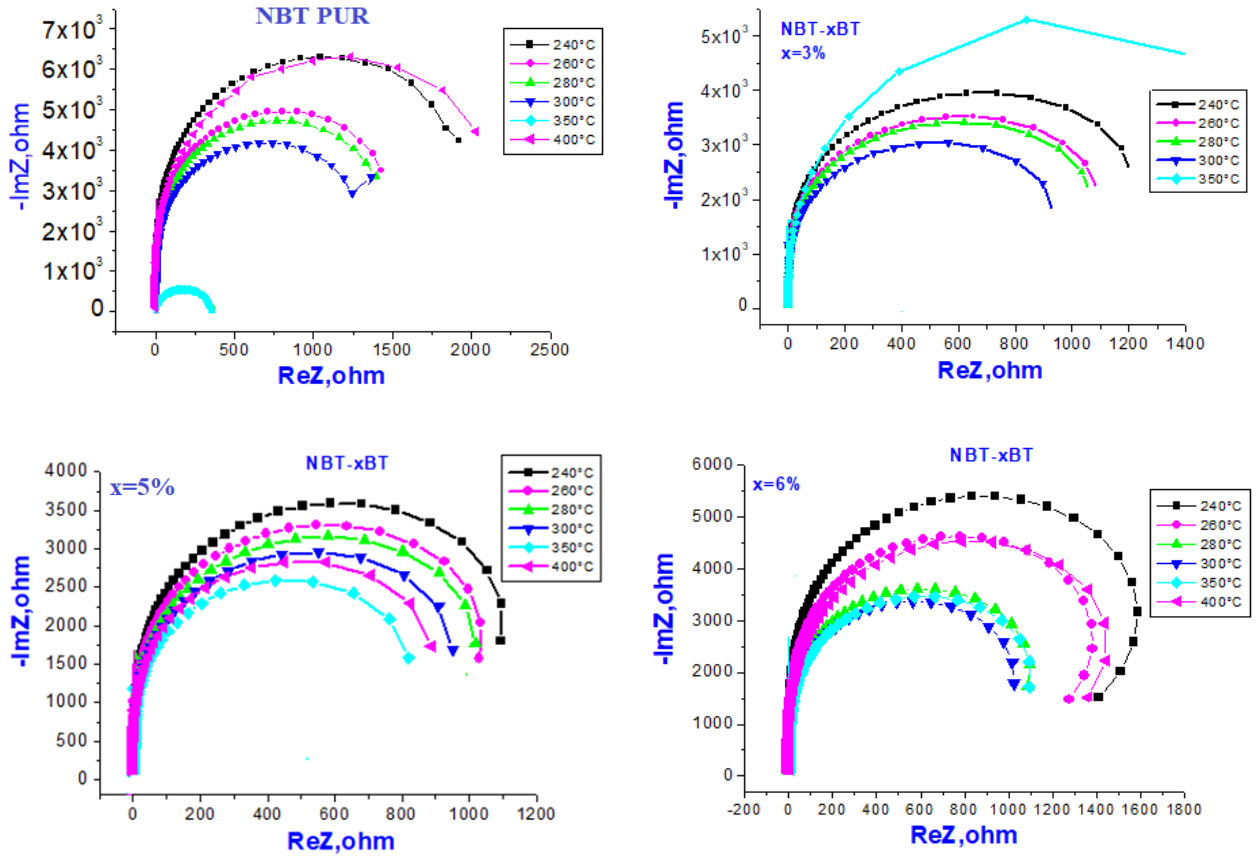

Figure 6. Plots of the imaginary part of the impedance (Im Z'') versus the real part (Z') at different temperatures for the (1-x)NBT-xBT system.

continue on the next page ...

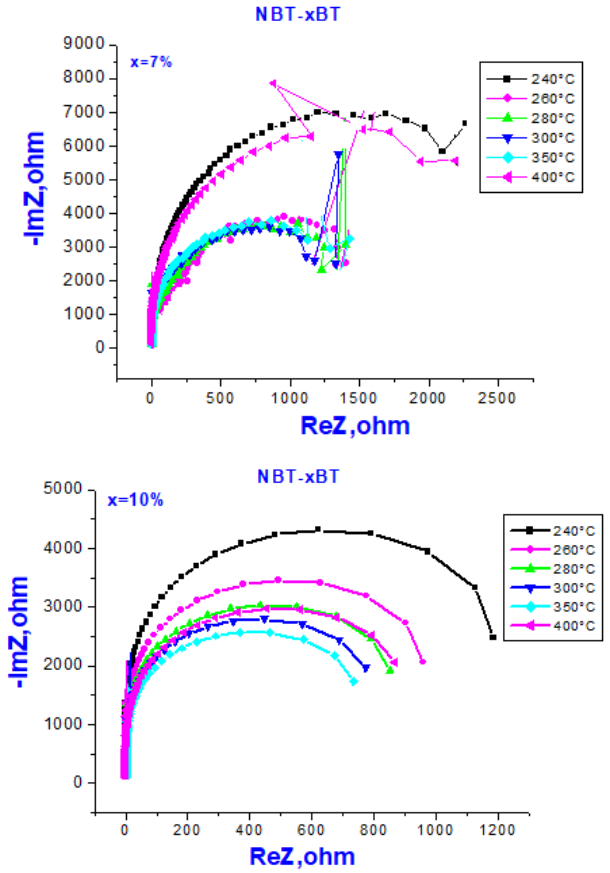

Figure 6. Plots of the imaginary part of the impedance (Im Z'') versus the real part (Z') at different temperatures for the (1-x) NBT-xBT system.

Table 6. Values of the grain strength (*Rg*), grain boundary strength (*Rgb*), relaxation frequency (*fr*), grain capacitance (*Cg*) and grain boundary capacitance (*Cgb*) of (1-x)NBT-xBT.

Temperature (°C)	Rg (KΩ)	Rgb (KΩ)	Cg (pF)	Cgb (pF)
NBT	10.45	4.23	1.21	0.09
x = 0.03	6.51	2.31	1.58	0.44
x = 0.05	6.17	2.02	1.51	0.34
x = 0.06	7.89	3.17	1.62	0.56
x = 0.07	8.73	3.95	1.71	0.93
x = 0.08	5.29	1.23	1.49	0.25
x = 0.10	5.97	1.96	1.41	0.29

These results confirm the observations made on the *ReZ'* and *ImZ''* spectra as a function of frequency for different temperatures. As T = 350 °C is overcome, the resistance R of the samples increases slightly, indicating a considerable decrease in the electrical conductivity. [30] It is also seen that the semi-circular arcs decrease with the variation in the xBT composition for a given temperature at T = 300 °C (Figure 7). The values of the fitted parameters (*Rb*, *Rgb*, *Cb* and *Cgb*) are grouped in Table 6 for all the samples at T = 300 °C. Therefore, a change in the strength/reactance ratio is observed with an increasing $BaTiO_3$ content.

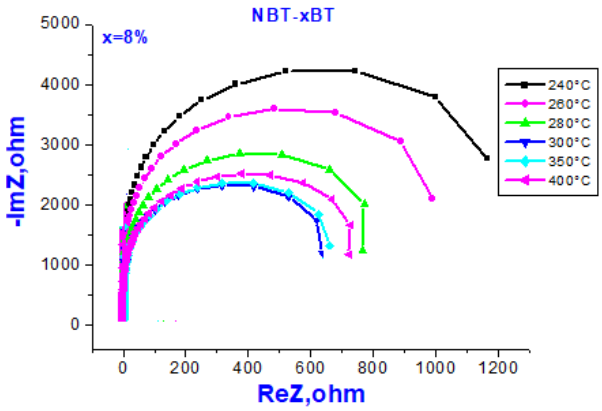

CONCLUSION

(1-x)NBT-xBT with (0.00 ≤ x ≤ 0.10) ceramics were examined. The structure refinements revealed that incorporation of x = 0.0 up to 3 % does not appear to change the chemical composition of the structure. However, for introduction of 8 % Ba^{2+}, the symmetry changes from the rhombohedral R3c structure to the tetragonal P4bm structure, by passing through a biphasic structure around the morphotropic phase boundary (MPB) for (x = 5 % up to x = 7 %). The dielectric studies show two anomalies noted, as A and B, as a function of the frequency for all the samples, corresponding to the so-called resonance frequency (*fr*) in A and for a frequency close to the anomaly B the frequency is called anti-resonance (*fa*). We report that as a function of the introduction of the xBa^{2+} content, an increase in the value of the dielectric permittivity is observed. However, beyond the morphotropic phase boundary (MPB), the maximum dielectric permittivity decreases for the xBa^{2+} rich region (x = 8 % and 10 %). Consequently, the relaxation frequency (f_{max} = 1/τ) depends on both the temperature and the xBT composition. Complex impedance spectroscopy was performed over a wide frequency range (500 − 2 MHz) at various temperatures

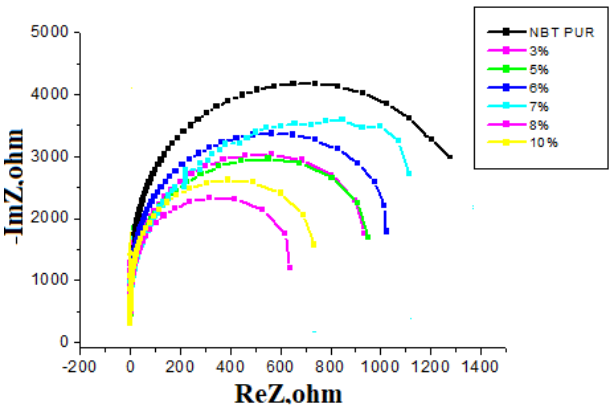

Figure 7. Evolution of -ImZ vs ReZ as a function of the xBT doping content.

to better understand the electrical properties and their correlation with the microstructure of the materials. A non-Debye mechanism was found with our materials. The Cole-Cole diagrams are fitted with an equivalent circuit based on the model of resistance in parallel with a capacitor to obtain the resistance and capacitance of the grains and grain boundaries of our material.

Acknowledgment

The authors would like to thank the Innovation Centre of the University of Fez for their assistance and support in processing the samples in this work. The authors would like to sincerely thank the anonymous reviewers for their careful proofreading and valuable comments on the paper.

REFERENCES

1. Haertling G. H. (1999): Ferroelectric ceramics: history and technology. *Journal of the American Ceramic Society, 82*(4), 797-818.doi: 10.1111/j.1151-2916.1999.tb01840.x
2. Mesrar M., Lamcharfi T., Echatoui N., Abdi F., Harrach A., Ahjyaje F. Z. (2019): Hydrothermal synthesis, microstructure and electrical properties of (1-x)($Na_{0.5}Bi_{0.5}$)$TiO_{3-x}BaTiO_3$ ceramics. *Moroccan Journal of Quantitative and Qualitative Research, 1*(1), 14-24.
3. Aksel E., Forrester J. S., Kowalski B., Deluca M., Damjanovic D., Jones J. L. (2012): Structure and properties of Fe-modified $Na_{0.5}Bi_{0.5}TiO_3$ at ambient and elevated temperature. *Physical Review B, 85*(2), 024121.doi: 10.1103/PhysRevB.85.024121
4. Mrharrab L., Nfissi A., Ababou Y., Belhajji M., Sayouri, S., Faik A. (2021): Effect of starting materials on the structure of pure and Gd-doped $BaTiO_3$ elaborated by the sol gel process. *Moroccan Journal of Chemistry, 9*(4), 9-4. doi: 10.48317/IMIST.PRSM/morjchem-v9i4.27263
5. Smolensky G. A. (1961): New ferroelectrics of complex composition. IV. *Sov. Phys.-Solid State, 2*, 2651-2654.
6. Shrout T. R., Zhang S. J. (2007): Lead-free piezoelectric ceramics: Alternatives for PZT?. *Journal of Electroceramics, 19*(1), 113-126.doi: 10.1007/s10832-007-9047-0
7. Devi C. S., Suresh M. B., Kumar G. S., Prasad G. (2016): High-temperature complex impedance and modulus spectroscopic studies of doped $Na_{0.5}Bi_{0.5}TiO_3$-$BaTiO_3$ ferroelectric ceramics. *Ionics, 22*(12), 2363-2377. doi: 10.1007/s11581-016-1781-3
8. Kumari R., Ahlawat N., Agarwal A., Sanghi S., Sindhu M. (2017): Structural transformation and investigation of dielectric properties of Ca substituted ($Na_{0.5}Bi_{0.5}$)$_{0.95-}$ $-xBa_{0.05}Ca_xTiO_3$ ceramics. *Journal of Alloys and Compounds, 695*, 3282-3289. doi: 10.1016/j.jallcom.2016.11.200
9. Benyoussef M., Zannen M., Belhadi J., Manoun B., Dellis J. L., El Marssi M., Lahmar A. (2018): Dielectric, ferroelectric, and energy storage properties in dysprosium doped sodium bismuth titanate ceramics. *Ceramics International, 44*(16), 19451-19460. doi: 10.1016/j.ceramint.2018.07.182
10. Benyoussef M., Zannen M., Belhadi J., Manoun B., Dellis J. L., Lahmar A., El Marssi M. (2020): Complex impedance and Raman spectroscopy of $Na_{0.5}(Bi_{1-x}D_{yx})_{0.5}TiO_3$ ceramics. *Ceramics International, 46*(8), 10979-10991.doi: 10.1016/j.ceramint.2020.01.114
11. Mesrar M., Lamcharfi T., Echatoui N. S., Abdi F., Ahjyaje F. Z., Haddad M. (2019): Effect of barium doping on electrical and electromechanical properties of (1-x)($Na_{0.5}Bi_{0.5}$)TiO_{3-x} $BaTiO_3$. *Mediterranean Journal of Chemistry, 8*(3), 198-208. doi: 10.13171/10.13171/mjc8319050908mm
12. Mohanty H. S., Kumar A., Sahoo B., Kurliya P. K., Pradhan D. K. (2018): Impedance spectroscopic study on microwave sintered (1−x)$Na_{0.5}Bi_{0.5}TiO_{3-x}BaTiO_3$ ceramics. *Journal of Materials Science: Materials in Electronics, 29*(8), 6966-6977. doi: 10.1007/s10854-018-8683-2
13. Aman D., Abd El-Hafiz D. R., Ebiad M. A. (2018): Thermodynamic parameter for steam reforming reaction of biodiesel by-product using nano-sized perovskite catalysts. *Moroccan Journal of Chemistry, 6*(3), 6-3.doi: 10.48317/IMIST.PRSM/MORJCHEM-V6I3.6444.
14. Chourti K., Marchet, P., El Hafiane Y., Bendahou A., El Barkany S., Karroua M., Abou-salama M. (2020): Relationships between crystalline structure and dielectric properties in $Sr_2Sm_{(1-x)}Nd_xTi_2Nb_3O_{15}$ ceramics. *Moroccan journal of chemistry, 8*(1), 304-317. doi: 10.48317/IMIST.PRSM/morjchem-v8i1.18479
15. East J., Sinclair D. C. (1997): Characterization of ($Bi_{1/2}Na_{1/2}$)TiO_3 using electric modulus spectroscopy. *Journal of Materials Science Letters, 16*(6), 422-425. doi: 10.1023/A:1018531419501
16. Kaswan K., Agarwal A., Sanghi S., Singh O. (2015):. Rietveld refinement and dielectric properties of ($Na_{0.5}Bi_{0.5}TiO_3$)-($Bi_{0.8}Ba_{0.2}FeO_3$) ceramics. In: *AIP conference proceedings* (Vol. 1665, No. 1, p. 140014). AIP Publishing LLC. doi: 10.1063/1.4918223
17. Pennington W. T. (1999): DIAMOND – Visual Crystal Structure Information System (software review), *Journal of Applied Crystallography, 32* (5), 1028–1029. doi: 10.1107/s0021889899011486
18. Jones G. O., Thomas P. A. (2002): Investigation of the structure and phase transitions in the novel A-site substituted distorted perovskite compound $Na_{0.5}Bi_{0.5}TiO_3$. *Acta Crystallographica Section B: Structural Science, 58*(2), 168-178. doi: 10.1107/S0108768101020845
19. Glazer, A. M. (1972). The classification of tilted octahedra in perovskites. *Acta Crystallographica Section B: Structural Crystallography and Crystal Chemistry, 28*(11), 3384-3392. doi:10.1107/S0567740872007976
20. Elbasset A., Sayouri S., Abdi F., Lamcharfi T., Mrharrab L. (2017): Effect of Sr addition on piezoelectric properties and the transition temperature of $BaTiO_3$. *Glass physics and chemistry, 43*(1), 91-97.doi: 10.1134/S1087659617010059
21. Belhajji M., Moutaouaffiq A., Nfissi A., Sayouri S., Lamcharfi T. D. (2022): Investigation of the structural, microstructural, and dielectric properties of Ho-doped $PbTiO_3$ for piezoelectric applications. *Journal of Materials Science: Materials in Electronics, 33*(1), 505-521. doi: 10.1007/s10854-021-07323-1
22. Damjanovic D. (1998): Ferroelectric, dielectric and piezoelectric properties of ferroelectric thin films and ceramics. *Reports on Progress in Physics, 61*(9), 1267.doi: 10.1088/0034-4885/61/9/002
23. Suchanicz J., Kwapulinski J. (1995): X-ray diffraction study of the phase transitions in $Na_{0.5}Bi_{0.5}TiO_3$. *Ferroelectrics,*

165(1), 249-253.doi: 10.1080/00150199508228304.
24. Mesrar M., Lamcharfi T., Echatoui N., Abdi F., Harrach A. (2018): Investigation of Morphotropic Phase Boundary by Rietveld refinement and Raman Spectroscopy for (1-x)($Na_{0.5}Bi_{0.5}$)TiO_3-x$BaTiO_3$ Ceramics. Asian Journal of Chemistry, 30(5), 1012-1018.doi: 10.14233/ajchem.2018.21116
25. Raghavender M., Kumar G. S., Prasad G. (2009): A-site substitution-controlled dielectric dispersion in lead-free sodium bismuth titanate. *Pramana, 72*(6), 999-1009. doi: 10.1007/s12043-009-0092-x
26. Zuo R., Su S., Wu Y., Fu J., Wang M., Li L. (2008): Influence of A-site nonstoichiometry on sintering, microstructure and electrical properties of ($Bi_{0.5}Na_{0.5}$)TiO_3 ceramics. *Materials Chemistry and Physics, 110*(2-3), 311-315.doi: 10.1016/j.matchemphys.2008.02.007
27. Devi C. S., Suresh M. B., Kumar G. S., Prasad G. (2018): Microstructural and high temperature dielectric, ferroelectric and complex impedance spectroscopic properties of $BiFeO_3$ modified NBT-BT lead free ferroelectric ceramics. *Materials Science and Engineering: B, 228,* 38-44. doi: 10.1016/j.mseb.2017.11.005
28. Li Y. M., Liao R. H., Jiang X. P., Zhang Y. P. (2009): Impedance spectroscopy and dielectric properties of $Na_{0.5}Bi_{0.5}TiO_3$–$K_{0.5}Bi_{0.5}TiO_3$ ceramics. *Journal of Alloys and Compounds, 484*(1-2), 961-965.doi: 10.1016/j.jallcom.2009.05.087
29. Barick B. K., Mishra K. K., Arora A. K., Choudhary R. N. P., Pradhan D. K. (2011): Impedance and Raman spectroscopic studies of ($Na_{0.5}Bi_{0.5}$)TiO_3. *Journal of Physics D: Applied Physics, 44*(35), 355402. doi: 10.1088/0022-3727/44/35/355402
30. Hemalatha K. S., Sriprakash G., Ambika Prasad M. V. N., Damle R., Rukmani K. (2015): Temperature dependent dielectric and conductivity studies of polyvinyl alcohol-ZnO nanocomposite films by impedance spectroscopy. *Journal of Applied physics, 118*(15), 154103. doi: 10.1063/1.4933286